Chapter 4

Delafossite $CuAlO_2$ Nanoparticles with Electrocatalytic Activity toward Oxygen and Hydrogen Evolution Reactions

Jahangeer Ahmed and Yuanbing Mao*

Department of Chemistry, University of Texas – Pan American, Edinburg, Texas 78539, United States
***E-mail: yuanbing.mao@utrgv.edu. Tel: +1-956-665-2417.**

As a type of novel electrocatalytic materials, delafossite $CuAlO_2$ nanoparticles (NPs) with an average particle size of ~ 20 nm were synthesized by a facile ultrasonic synthesis followed with annealing at 850°C in N_2 for the first time. Their phase purity, size and morphology were investigated by powder X-ray diffraction, Raman spectroscopy and electron microscopic studies. Their electrochemical performance studies demonstrated promising catalytic activity in the electrolysis of water to the hydrogen evolution reactions (HER) and oxygen evolution reactions (OER) compared to bulk $CuAlO_2$. More specifically, these $CuAlO_2$ nanoparticles showed 12 times higher current density to the OER than the bulk counterpart. Hence, being a low-cost semiconducting material, these delafossite $CuAlO_2$ nanoparticles with the size of ~ 20 nm could be useful to further study their other applications like solar cells, photochemical water splitting, proton exchange membrane water electrolysis etc.

Liu and Bashir; Nanomaterials for Sustainable Energy
ACS Symposium Series; American Chemical Society: Washington, DC, 2015.

Introduction

To effectively address the fossil fuel depletion issue and serious environmental problems accompanying its combustion, new forms of energy that is clean, renewable, cheap, safe and viable are currently under intensive search. Hydrogen has received considerable attention recently as a next-generation energy carrier. Electrolysis of water with the assistance of catalysts provides hydrogen and oxygen which have a potential to provide sustainable energy via fuel cells. Hydrogen is used as a fuel in the fuel cells by converting the chemical energy into electrical energy and also used as a fuel in automobile and aerospace industries while oxygen is also useful in fuel cells to assist the power generation by enhancing the temperature of the reactors because of the completion of combustion reactions. However, efficient catalysts are still under intensive search for water splitting for good product selectivity from band alignment with chemical redox potentials, fast reaction kinetics from desirable efficiencies and without charge carrier recombination in addition to good stability, cost-effective and non-toxicity.

Delafossites with the general formula $A^{I}M^{III}O_2$ comprised of alternating layers of slightly distorted edge-shared MO_6 octahedra and two-dimensional close-packed A-cation planes forming linear O-A^{1+}-O "dumbbells", and the oxygens coordinated by 4 cations (1 A^{I} & 3 M^{III}) are important p-type transparent conducting oxide materials (*1*) which exhibits a variety of applications including gas sensors (*2*), optical (*3–7*), electrical (*5*, *8*, *9*) and thermoelectric devices (*10*), dilute magnetic semiconductors (*11*), field emission displays (*12*), photo-catalytic water splitting (*13*), and solar cells applications (*14–17*). Delafossites have been progressively studied in the last decade , especially after $CuAlO_2$ was discovered as a good *p*-type transparent conducting oxide (TCO) with high conductivity, and then attracted attention for *p*-type dye-sensitized solar cells (DSSCs) due to their desirable low valence band (VB) edge position and high hole mobility, almost exclusively on $CuMO_2$ with M = Al, Ga or Cr. Copper based delafossites with copper at the A–site have a wide variety of interesting electronic properties (*1*, *18*). Few examples of delafossites like $PtCoO_2$ (*19*), $PdCoO_2$ (*19*), $PdRhO_2$ (*19*), $CuRhO_2$ (*20*, *21*) have also been reported in literature as the electro-catalysts for oxygen evolution reaction (OER). There is only one report in the literature regarding the electrocatalysis based on delafossite $CuAlO_2$ (*21*), and the electrochemical behavior of delafossite $CuAlO_2$ has not been studied extensively. Therefore, we are motivated to synthesize $CuAlO_2$ nanoparticles and study their electrochemical performance. Moreover, we demonstrated that these delafossite $CuAlO_2$ nanoparticles are promising catalysts in electrolysis of water to the hydrogen and oxygen evolutions.

High temperature (above 1000 °C) synthesis normally form micron–sized $CuAlO_2$ particles. Therefore, one of our aims was to synthesize $CuAlO_2$ nanoparticles in the nanometer region by lowering the synthesis temperature. In terms of the synthesis of delafossite $CuAlO_2$ nanoparticles, there are several used techniques including sol–gel (*3*, *14*, *22*, *23*), hydrothermal (*15*, *24*, *25*), mechanical alloying (*9*, *17*), pulsed laser deposition (*8*), sputtering (*12*, *26*), and electro-spinning (*7*) methods. Nanocrystalline $CuAlO_2$ particles were also

synthesized from a biological process at low temperature (50 °C) (*6*) and by using boehmite nanorods (γ-AlOOH) and copper (I) acetate as the precursor at high temperature (1150 °C) (*27*). At the meantime, bulk delafossite $CuAlO_2$ could be easily synthesized by solid state method at high temperature range from 1100 °C to 1200 °C (*27–29*).

To the best of our knowledge, there is no report in literature based on the ultrasonic synthesis of $CuAlO_2$ nanoparticles. Herein, we report a facile synthesis of $CuAlO_2$ nanoparticles (~20 nm) using the ultrasonic process followed by the annealing in N_2 atmosphere at 850 °C for 48 h. It is noteworthy that the ultrasonic process provides the smallest $CuAlO_2$ nanoparticles compared with reported data on the literature based on our best knowledge. The smallest $CuAlO_2$ nanoparticles previously reported were in the range from 35 nm to 50 nm by using chemical routes (*3*, *14*, *27*). Furthermore, we carefully investigate the electrochemical performance of $CuAlO_2$ nanoparticles to the OER and HER by electrolysis of water using 0.5 M KOH and Ag/AgCl as the electrolyte and reference electrode, respectively. The structural and morphological characterizations of the nanopowders were investigated by powder X-ray diffraction (PXRD), Raman spectroscopy, field emission scanning electron microscopy (FESEM), transmission electron microscopy (TEM), and energy dispersive x–ray studies.

Experimental

Materials and Synthesis Methods

$Cu(NO_3)_2•3H_2O$ (Sigma Aldrich, 99 %), $Al(NO_3)_3•3H_2O$ (Sigma Aldrich, 98 %), and $NaHCO_3$ (Sigma Aldrich, 99.7 %) were used in the ultrasonic synthesis of the $CuAlO_2$ nanoparticles. The ultrasonic process involved the mixing of parent materials (0.1 M $Cu(NO_3)_2•3H_2O$ and 0.1 M $Al(NO_3)_3•3H_2O$) followed by the titration with 0. 5 M $NaHCO_3$ aqueous solution drop by drop at 25 °C under the ultrasonic wave (operating at 117 V with the frequency of 60 kHz) and kept for 3 h. The light green precipitates were centrifuged followed by washing with deionized water for three times. The resulting light green colored powders were then dried at 60 °C for 6 h and used as a precursor in the synthesis of grey colored $CuAlO_2$ nanoparticles at 850 °C for 48 h in N_2 (99.999 %). Bulk counterpart, i.e. $CuAlO_2$ micron sized particles, were also synthesized via solid state route to compare the electrochemical performance with the $CuAlO_2$ nanoparticles. More specifically, Al_2O_3 (Sigma Aldrich, 98%) and CuO nanopowders (size ~50 nm, Sigma Aldrich) were taken at 1:2 molar ratio and ground together for half an hour in an agate mortar pestle followed by firing at 1150 °C for 36 h in N_2 atmosphere.

Materials Characterization

The resulting products of both cuprous aluminate delafossite [$CuAlO_2$] nanoparticles and bulk counterpart were initially characterized by powder X-ray diffraction (PXRD) spectroscopy carried out on a Bruker D8 Advanced diffractometer with Ni-filtered Cu-Kα radiation (λ = 1.5406 Å) in the 2θ range from 10° to 60° with the scan rate of 0.02°/second on a zero background sample

holder. Raman scattering experiments were carried out by a Bruker SENTERRA RAMAN microscope with a 785 nm Ar^+ laser as the excited light and an objective of 20X of optical microscope. The laser beam was focused to a spot size of 5 μm with the power of 10 mW. Both the particle size and morphology of the $CuAlO_2$ nanoparticles were investigated by the ZEISS SIGMA VP FESEM and ZEISS LEO 900 TEM operated at 5 kV and 80 kV, respectively. The TEM samples were prepared by the dispersion of 2 mg of the nanoparticles in 10 ml of ethanol under the ultra-sonication for 5 min and a drop of suspension was placed on to the surface of porous carbon film supported by a copper grid followed by drying in air. Thermo-gravimetric analysis (TGA) of the nanomaterials was carried out using a Perkin–Elmer system with a heating rate of 10 °C/min in oxygen atmosphere.

Electrochemical Measurements

Electrolysis of water for gas (O_2 and H_2) evolutions was carried out with a computer controlled potentiostat/galvanostat (Metrohm Autolab B.V.) at room temperature. The electrochemical work station contains three electrodes, i.e. Pt wire, Ag/AgCl, and glassy carbon electrodes as the counter electrode, reference electrode and working electrode, respectively. The working electrodes were prepared by pasting $CuAlO_2$ powders with carbon black and polyvinylidene fluoride (PVDF, weight fractions of $CuAlO_2$:carbon black:PVDF of 75:15:10 w/w) on to the surface of glassy carbon electrode followed by drying at 65 °C in vacuum oven. The prepared electrodes were used as the working electrodes in the electrochemical measurements, including cyclic voltammetry (CV) and chronoamperometry, for oxygen evolving reaction (OER) and hydrogen evolution reactions (HER). Cyclic voltammetry was carried at the scan rate of 5, 10, 25, 50 and 100 mV/s versus Ag/AgCl electrode for the OER and from 0 to -1.2 V versus the Ag/AgCl electrode for the HER in alkaline electrolyte (0.5 M KOH). Chronoamperometric measurements were carried out for 200 s at 0.60 V and -1.2 V versus Ag/AgCl for OER and HER, respectively, in 0.5 M KOH electrolyte. The nitrogen gas was passed through the electrolyte for 10 minutes prior to the electrochemical measurements to remove the dissolved air from the electrolyte toward the OER and HER. Also electrochemical measurements in O_2–saturated 0.5 M potassium (I) hydroxide (KOH) were run for OER. All measurements to study the OER and HER were conducted with freshly prepared electrodes and electrolytes. The current density of the $CuAlO_2$ electrocatalysts was calculated using the electro-active surface area of electrode which is calculated by using the Randles–Sevcik equation (*30–32*).

Results and Discussion

Materials Characterization

Based on the powder X-ray diffraction pattern, the as-synthesized precursor after the ultrasonic process could be analyzed on the basis of crystalline phases of basic copper carbonate ($Cu_2(OH)_2CO_3$) and aluminum (III) hydroxide ($Al(OH)_3$) (Figure 1a). The annealing of this precursor in N_2 atmosphere at 850 °C for

48 h leaded to the formation of grey monophasic copper aluminate ($CuAlO_2$) nanoparticles (Figure 1b). Figure 1c shows the PXRD pattern of $CuAlO_2$ bulk particles obtained by solid state route, which cannot be synthesized at or below 1000 °C, either in air or inert atmosphere (*28*, *29*). All the reflections (003, 006, 101, 012, 104, 009, 107 and 018) could be indexed on the basis of pure phase of rhombohedral structure with space group of R3-m (JCPDS file # 01-075-2356).

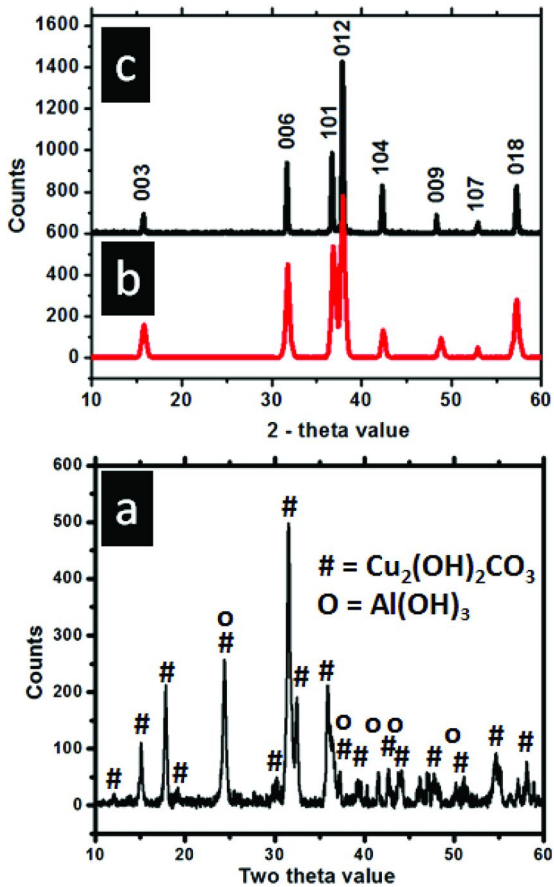

Figure 1. PXRD patterns of (a) the as-synthesized precursor by ultrasonic process at room temperature, (b) the $CuAlO_2$ nanoparticles obtained subsequently at 850 °C for 48h in N_2, and (c) bulk $CuAlO_2$ particles synthesized by solid state route at 1150 °C for 36 h.

Figure 2 shows the FESEM and TEM micrographs of the synthesized $CuAlO_2$ nanoparticles and the bulk counterpart. The FESEM and TEM studies (Figures 2a and 2b) showed the formation of spherical shaped nanoparticles with an average particles size of ~20 nm. By considering the reported particle size of $CuAlO_2$ nanoparticles (*3*, *14*, *27*), what presented here obtained by the ultrasonic process followed by firing at 850 °C has the smallest size. Specifically, $CuAlO_2$ nanoparticles reported recently on the literature with the smallest average size (35 nm) were prepared by an acid catalyzed sol–gel method followed by the heat treatment in sealed silica tube under a controlled partial pressure (p) of oxygen (pO_2) of 10^{-5} atm (*14*). Figure 2c shows the FESEM image of bulk $CuAlO_2$ with micron–sized plates-like particles (~2 μm) which were synthesized by the solid state route at 1150°C. From Brunauer, Emmett and Teller (BET) surface area measurements, the specific surface area of the $CuAlO_2$ nanoparticles and $CuAlO_2$ bulk particles were found to be 1.15 and 0.025 m^2/g, respectively. As expected, the specific BET surface area increases with decreasing the particle size of these $CuAlO_2$ particles. As reported in the literature, delafossite $CuAlO_2$ nanoparticles are an important transparent semiconducting oxides for the light to electricity conversion in dye-sensitized solar cells (DSSCs). The conversion efficiencies depend not only on the nature of semiconducting materials and dye molecules but also on semiconducting particle size with uniform distribution (*14–17*). Therefore, the synthesized $CuAlO_2$ nanoparticles here with the smallest particle size of ~20 nm could be an ideal choice for further studies of their various applications, including the electrocatalytic performance studied here.

The rhombohedral crystal structure of the $CuAlO_2$ samples were also characterized using Raman spectroscopy. Figure 3 shows Raman spectra of the rhombohedral $CuAlO_2$ nanoparticles which were collected by employing the normal backscattering geometries. The Raman active modes (E_g and A_{1g} modes) of rhombohedral $CuAlO_2$ with R3-m space group could be summarized according to the following equation (irreducible representation Γ): $= E_g + A_{1g}$, where the A_{1g} mode has atomic vibrations in the direction of c-axis along the O–Cu–O bonds and the E_g mode describes the atomic vibrations perpendicular to c-axis (*33–35*). In the Raman spectrum of the $CuAlO_2$ nanoparticles, only two sharp bands were observed at 415 and 760 cm^{-1}, which could be assigned to Raman active E_g and A_{1g} modes, respectively, of the rhombohedral crystal structure of delafossite $CuAlO_2$. Its A_{1g} Raman active mode is slightly shifted when compared to the bulk $CuAlO_2$ particles, which appears at 764 cm^{-1}. As reported on pressure and temperature dependent Raman studies in the literature, the frequencies of Raman active modes (E_g and A_{1g}) of delafossite $CuAlO_2$ nanoparticles can be compared with those of bulk $CuAlO_2$, of which the phonon modes of E_g and A_{1g} were reported at 418 and 767 cm^{-1}, respectively (*33*, *35*). Even though the specific reason needs further studies, the shift in the phonon modes from the $CuAlO_2$ nanoparticles could be explained on the basis of thermal expansion, lattice expansion, anharmonic phonon-phonon interaction, and polaronic effects with pressure and temperature (*33–35*).

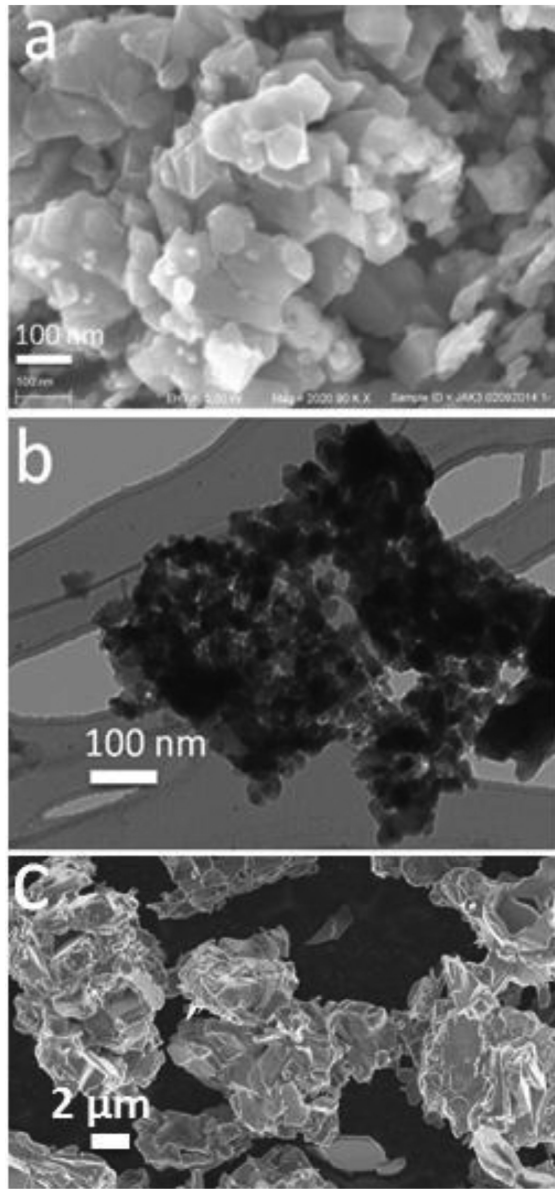

Figure 2. (a) FESEM and (b) TEM images of the $CuAlO_2$ nanoparticles. (c) FESEM image of the bulk $CuAlO_2$ particles.

Thermal studies of these $CuAlO_2$ nanoparticles could be useful to the research of their stability and in the preparation of their thin films at high temperature for various applications. Figure 4a shows the TGA plot of the $CuAlO_2$ nanoparticles under the flow of oxygen gas with the heating rate of 5 °C/min from 30 to 900 °C. A very small amount of weight loss occurs up to ~250 °C which could be due to the loss of adsorbed moisture by the nanoparticles. Subsequently, we observe that the $CuAlO_2$ nanoparticles demonstrate no obvious weight change up to 675 °C in O_2 atmosphere. Thermal studies of $CuAlO_2$ nanoparticles up to this temperature (~675°C) confirm the absence of O_2 deficiency in this material (*14*). Hereafter, the weight increases and that could be attributed the beginning of decomposition of the $CuAlO_2$ nanoparticles to CuO and $CuAl_2O_4$ (*14*). Powder X-ray diffraction studies of the residual material confirm the complete decomposition of the $CuAlO_2$ nanoparticles at 900 °C in O_2 (Figure 4b). Our results also agree with other previous reports (*14*, *28*, *29*).

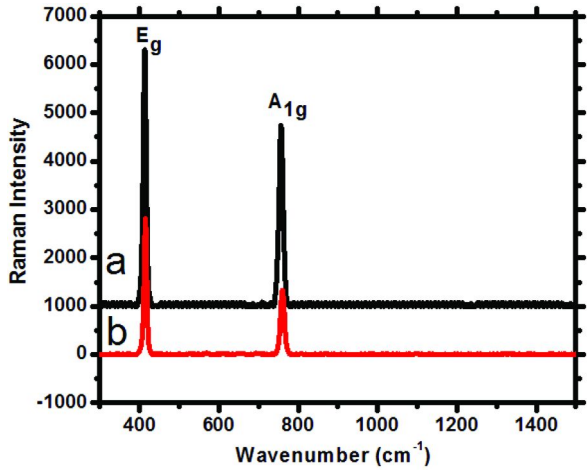

Figure 3. Raman spectra of (a) the $CuAlO_2$ nanoparticles and (b) the bulk $CuAlO_2$ particles.

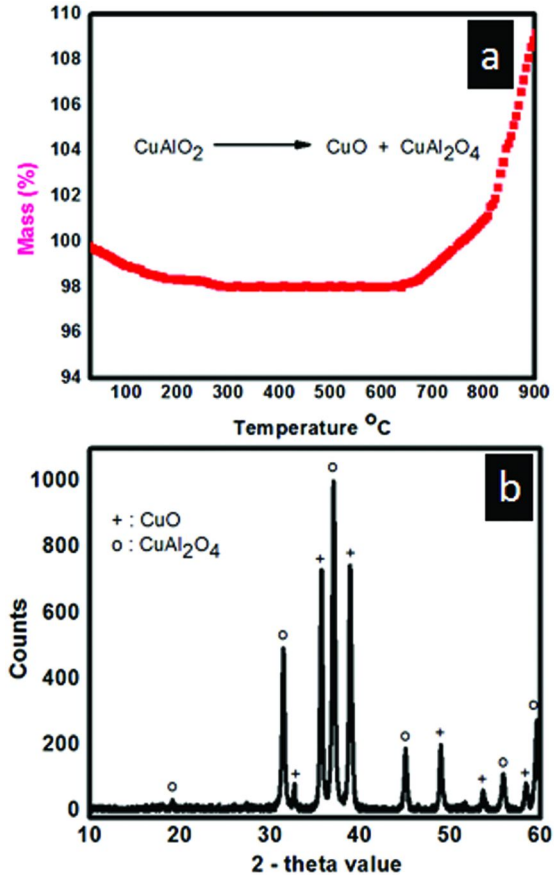

Figure 4. (a) TGA study of the $CuAlO_2$ nanoparticles in oxygen. (b) PXRD patterns of the product obtained after the TGA study in oxygen.

Electrocatalytic Performance

The electro-chemical measurements (cyclic voltammetry, CV) and chrono-amperometric, CA)) were carried out for the HER and OER using 0.5 M KOH electrolyte and Ag/AgCl reference electrode by passing N_2 gas in the electrolyte for 5 min before starting the electrolysis of water. Figure 5a and 5b show the CV curves of the $CuAlO_2$ nanoparticle and bulk particles for HER from –1.2 to 0.4 V versus Ag/AgCl while figure 6c and 6d show their CV curves for OER from –0.1 to 1.0 V versus Ag/AgCl at the scan rates of 5, 10, 25, 50, 100 mV/s. Cyclic voltammograms (Figure 5a and 5b) show a redox peak around –0.20 V which could be assigned to the Cu^+ to Cu^{2+} conversion as reported in the literature (*36*, *37*). From the CV studies at various scan rates, i.e. from 5 to 100 mV/s, the $CuAlO_2$ nanoparticles generate slightly higher current than the bulk $CuAlO_2$ particles for the HER. From Randles–Sevcik equation (*30–32*), the current density of the $CuAlO_2$ nanoparticles was found to be slightly higher (64

mA/cm^2) than that of the bulk $CuAlO_2$ particles (61 mA/cm^2) calculated by using the electrode electroactive surface area of 0.0786 cm^2. The current density could be a combination of both faradaic and non-faradaic processes and a function of the surface area and the morphology of the electrode materials. In the faradaic process, the charge transferred across the electrode–electrolyte which is governed by Faraday's law. Herein, electrons transferred from electrocatalysts to water molecules to generate hydroxide ion and hydrogen according to the following reaction: $2H_2O + 2e^- \rightarrow H_2 + 2OH^-$. Noticeably, there is no report in literature on HER by the electrolysis of water using delafossite $CuAlO_2$ as an electrocatalyst while copper based materials including intermetallic (Cu-Co) (*37*), Cu_2O (*38*), Cu (*36*) were used as electrocatalysts in hydrogen generation. As shown here, delafossite $CuAlO_2$ shows an enhancement in the generation of hydrogen from the electrolysis of water compared to the other copper based materials. Figure 5c and 5d show the CV curves of $CuAlO_2$ nanoparticles and bulk $CuAlO_2$ particles, respectively, for OER at the various scan rates from 5 to 100 mV/s in 0.5 M KOH versus Ag/AgCl.

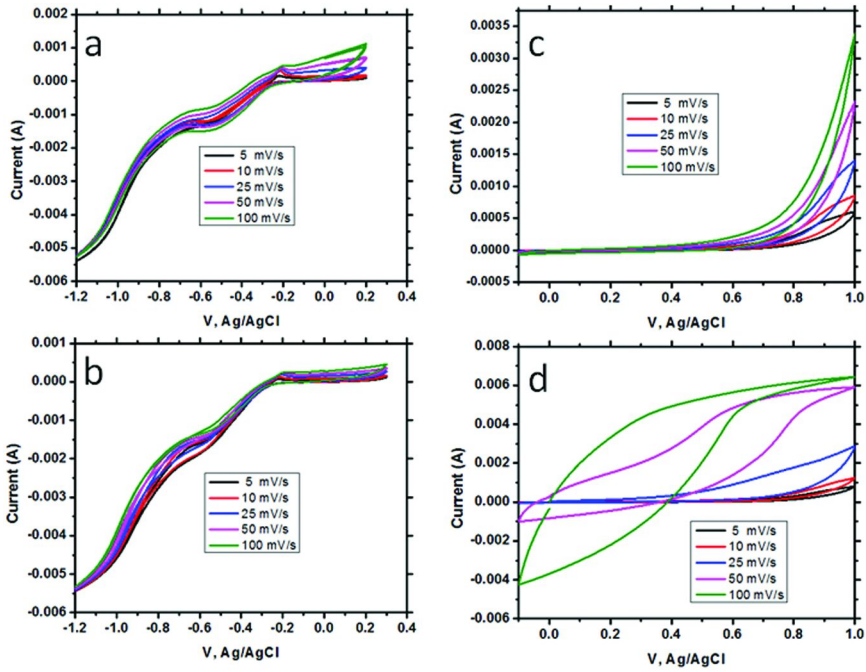

Figure 5. Cyclic voltammetry of (a) the $CuAlO_2$ nanoparticles and (b) the bulk $CuAlO_2$ particles for HER at various scan rates, and (c) the $CuAlO_2$ nanoparticles and (d) the bulk $CuAlO_2$ particles for OER at various scan rates.

Chronoamperometry (CA) is a potentiostatic true quantitative measurement which is used to investigate the electrocatalytic performance of the materials at the fixed potential. The charge transfer processes were also studied by CA experiments using these $CuAlO_2$ samples as electrocatalysts for HER and

OER (Figure 6). Insets of Figures 6a and 6b reveal the schematic diagrams of electrochemical cell and cell reactions occur at the surface of working electrodes to the HER and OER from the electrolysis of water. Figure 6a shows the CA experiments of the $CuAlO_2$ electrocatalysts for the HER at the fixed potential of –1.2 V for 200 seconds. In our experiment, the electrochemical reaction stops when the potential is switched off and hence current drops drastically. From the CA measurements, the nanocrystalline $CuAlO_2$ particles generate slightly higher current than the bulk $CuAlO_2$ particles (Figure 6a). The cathodic current generated is directly proportional to the rate of hydrogen evolution. The current densities were found to be 67 mA/cm^2 and 64 mA/cm^2 for the nanosized and bulk $CuAlO_2$ particles, respectively, which are consistent with the current density observed by CV measurements in Figure 6. A slightly higher current density clearly indicates that the $CuAlO_2$ nanoparticles are showing better performance than the bulk $CuAlO_2$ particles in the electrolysis of water to HER. This is noteworthy that the delafossite $CuAlO_2$ particles have been showing a promising electrocatalytic behavior to the HER. Figure 6b shows the CA measurements of the nanosized and bulk $CuAlO_2$ particles for the OER at the fixed potential of 0.60 V for 200 seconds. By comparing the catalytic activity of these electrodes in CA, we clearly observe that the nanosized $CuAlO_2$ particles generate higher current than the bulk $CuAlO_2$ particles up to 200 seconds. The current densities for the nanosized $CuAlO_2$ nanoparticles (14 mA/cm^2) and bulk $CuAlO_2$ particles (1.13 mA/cm^2) were calculated by using the electroactive surface area of the electrode. The electroactive surface area of the electrode (nanosized particles = 0.053 cm^2, bulk particles = 0.133 cm^2) for OER was calculated by using Randles–Sevcik equation. In the present study, we found that the nanosized $CuAlO_2$ particles show much better electrocatalytic activity (12 times) than the bulk particles toward the OER.

We have also investigated the catalytic efficiencies of the delafossite $CuAlO_2$ samples in O_2–saturated electrolyte (0.5M KOH) versus Ag/AgCl to OER (Figure 7). These data show an enhancement with consistency of current generation at the various scan rates (from 10–100 mV/s). Figure 7a and 7b show the CV curves of $CuAlO_2$ nanoparticles and bulk particles. From the CV studies, we observe that the OER starts beyond the potential of 0.5 V in both cases and the current generated is consistent with the $CuAlO_2$ nanoparticles in the O_2–saturated electrolyte versus Ag/AgCl compared to the bulk materials. $CuAlO_2$ nanoparticles generate higher current than the bulk particles in O_2–saturated 0.5M KOH compared to the N_2–saturated 0.5 M KOH to the OER which is also consistent with the CA studies (Figure 7c). The electroactive surface area of the nanoparticles (0.114 cm^2) and bulk particles (0.046 cm^2) of $CuAlO_2$ was used to calculate the current density. The observed current density of the $CuAlO_2$ nanoparticles (17.5 mA/cm^2) to OER was found to be higher than the bulk particles (10.8 mA/cm^2) in O_2–saturated 0.5 M KOH electrolyte. Therefore, the present work demonstrated that the $CuAlO_2$ nanoparticles are promising electrocatalysts to the HER and OER in alkaline electrolyte versus Ag/AgCl and show enhanced catalytic activity compared to the bulk counterpart.

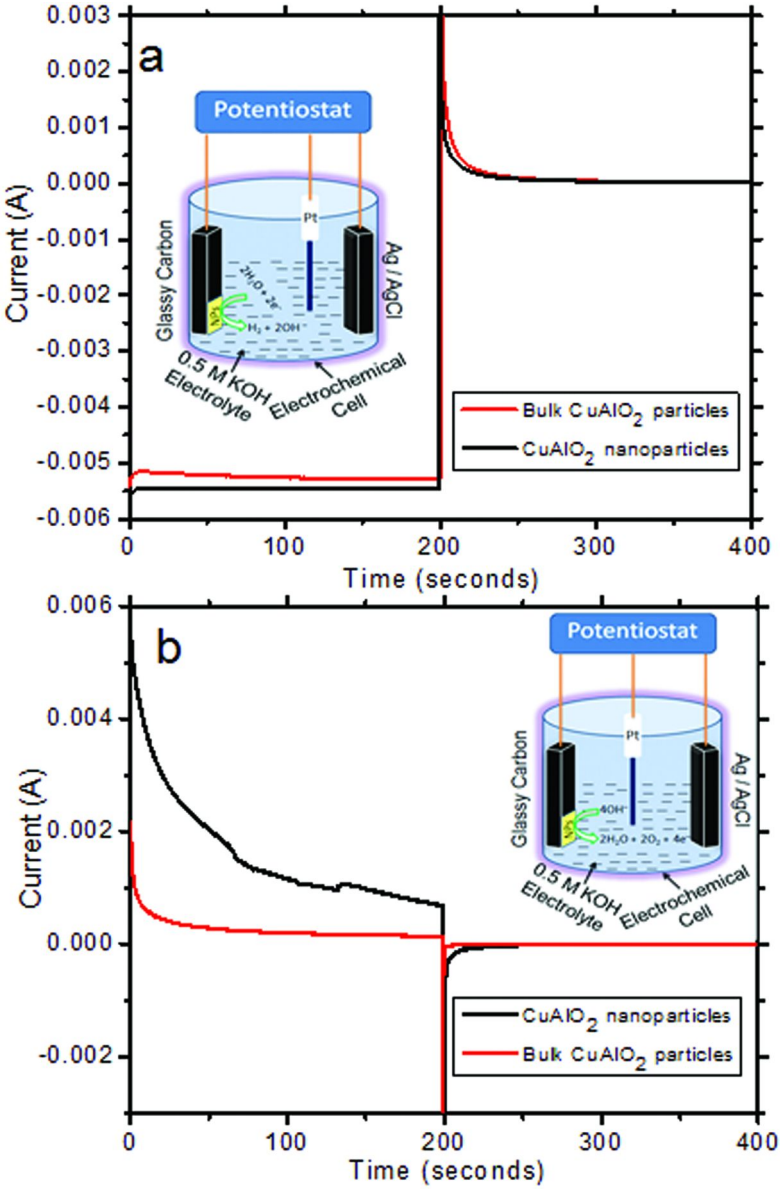

Figure 6. Chronoamperometry of the $CuAlO_2$ nanoparticles and bulk $CuAlO_2$ particles for (a) HER at -1.2 V vs Ag/AgCl and (b) OER at 0.6 V vs Ag/AgCl. Insets of Figures 6a and 6b represent the schematic diagrams of HER and OER, respectively.

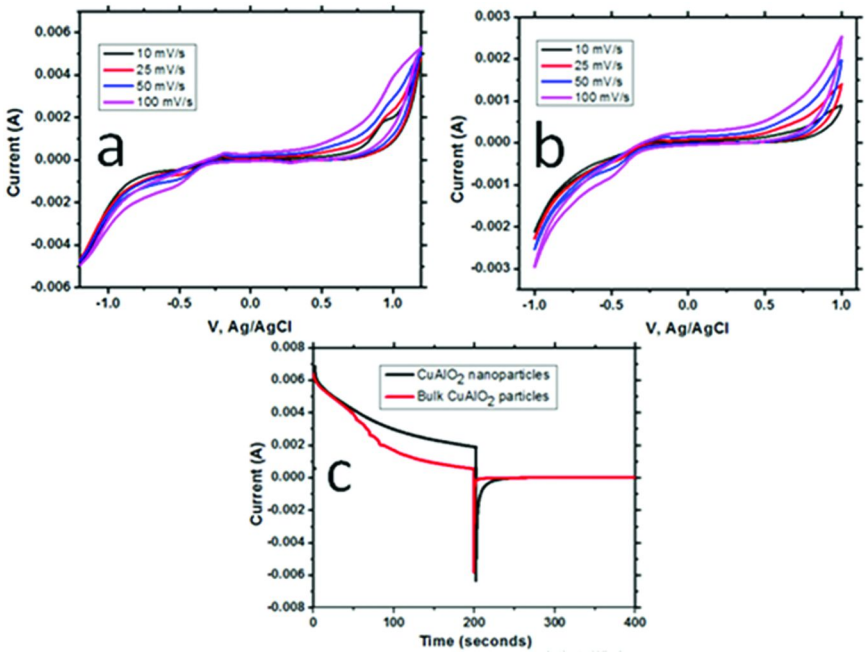

Figure 7. Cyclic voltammetry of (a) the $CuAlO_2$ nanoparticles and (b) the bulk $CuAlO_2$ particles for OER at various scan rates in O_2–saturated 0.5 M KOH. (c) Chronoamperometry of the $CuAlO_2$ nanoparticles and bulk particles for OER in O_2–saturated 0.5 M KOH at 0.6 V versus Ag/AgCl.

Conclusions

Herein, we report the synthesis of $CuAlO_2$ nanoparticles with average size of ~20 nm for the first time via an ultrasonic process followed with annealing at 850 °C in N_2. The phase purity of the $CuAlO_2$ nanoparticles was investigated by powder X-ray diffraction and Raman spectroscopic studies while their morphology was studied by SEM and TEM. More importantly, it was found that the $CuAlO_2$ nanoparticles show higher electrocatalytic activity than the micron-sized particles toward the hydrogen and oxygen evolution reactions in 0.5 M KOH electrolytes versus Ag/AgCl. Therefore, these results confirmed that delafossite $CuAlO_2$ can serve as promising electrocatalyst for water splitting and will draw intensive research interest on their other applications like solar cells, photochemical water splitting, proton exchange membrane water electrolysis etc.

Acknowledgments

The authors thank the support from the American Chemical Society – Petroleum Research Fund #51497, the Air Force Office of Scientific Research (award # FA9550-12-1-0159), and the National Science Foundation under DMR grant # 0934157 (PREM-UTPA/UMN-Science and Engineering of Polymeric and

Nanoparticle-based Materials for Electronic and Structural Applications). The authors also thank to Dr. M. Pokhrel for taking SEM images, Ms. T. Olmedo for taking TEM images, and Ms. J. Cruz for performing BET measurements.

References

1. Kawazoe, H.; Yasukawa, M.; Hyodo, H.; Kurita, M.; Yanagi, H.; Hosono, H. P-type electrical conduction in transparent thin films of $CuAlO_2$. *Nature* **1997**, *389* (6654), 939–942.
2. Zheng, X. G.; Taniguchi, K.; Takahashi, A.; Liu, Y.; Xu, C. N. Room temperature sensing of ozone by transparent p-type semiconductor $CuAlO_2$. *Appl. Phys. Lett.* **2004**, *85* (10), 1728–1729.
3. Mo, R.; Liu, Y. Synthesis and properties of delafossite $CuAlO_2$ nanowires. *J. Sol-Gel Sci. Technol.* **2011**, *57* (1), 16–19.
4. Banerjee, A. N.; Chattopadhyay, K. K. Size-dependent optical properties of sputter-deposited nanocrystalline p-type transparent $CuAlO_2$ thin films. *J. Appl. Phys.* **2005**, *97* (8), 084308.
5. Li, G.; Zhu, X.; Lei, H.; Jiang, H.; Song, W.; Yang, Z.; Dai, J.; Sun, Y.; Pan, X.; Dai, S. Preparation and characterization of $CuAlO_2$ transparent thin films prepared by chemical solution deposition method. *J. Sol-Gel Sci. Technol.* **2010**, *53* (3), 641–646.
6. Ahmad, A.; Jagadale, T.; Dhas, V.; Khan, S.; Patil, S.; Pasricha, R.; Ravi, V.; Ogale, S. Fungus-based synthesis of chemically difficult-to-synthesize multifunctional nanoparticles of $CuAlO_2$. *Adv. Mater.* **2007**, *19* (20), 3295–3299.
7. Zhao, S.; Li, M.; Liu, X.; Han, G. Synthesis of $CuAlO_2$ nanofibrous mats by electrospinning. *Mater. Chem. Phys.* **2009**, *116* (2–3), 615–618.
8. Yanagi, H.; Inoue, S.-i.; Ueda, K.; Kawazoe, H.; Hosono, H.; Hamada, N. Electronic structure and optoelectronic properties of transparent p-type conducting $CuAlO_2$. *J. Appl. Phys.* **2000**, *88* (7), 4159–4163.
9. Prakash, T.; Prasad, K. P.; Kavitha, R.; Ramasamy, S.; Murty, B. S. Dielectric relaxation studies of nanocrystalline $CuAlO_2$ using modulus formalism. *J. Appl. Phys.* **2007**, *102* (10), 104104.
10. Koumoto, K.; Koduka, H.; Seo, W.-S. Thermoelectric properties of single crystal $CuAlO_2$ with a layered structure. *J. Mater. Chem.* **2001**, *11* (2), 251–252.
11. Kizaki, H.; Sato, K.; Yanase, A.; Katayama-Yoshida, H. Ab initio calculations of $CuAlO_2$-based dilute magnetic semiconductor. *Phys. B* **2006**, *376–377*, 812–815.
12. Arghya Narayan, B.; Sang, W. J. Low-macroscopic field emission properties of wide bandgap copper aluminium oxide nanoparticles for low-power panel applications. *Nanotechnology* **2011**, *22* (36), 365705.
13. Smith, J. R.; Van Steenkiste, T. H.; Wang, X.-G. Thermal photocatalytic generation of H_2 over $CuAlO_2$ nanoparticle catalysts in H_2O. *Phys. Rev. B* **2009**, *79* (4), 041403.

14. Ahmed, J.; Blakely, C. K.; Prakash, J.; Bruno, S. R.; Yu, M.; Wu, Y.; Poltavets, V. V. Scalable synthesis of delafossite $CuAlO_2$ nanoparticles for p-type dye-sensitized solar cells applications. *J. Alloys Compd.* **2014**, *591*, 275–279.
15. Bandara, J.; Yasomanee, J. P. P-type oxide semiconductors as hole collectors in dye-sensitized solid-state solar cells. *Semicond. Sci. Technol.* **2007**, *22* (2), 20.
16. Nattestad, A.; Zhang, X.; Bach, U.; Cheng, Y.-B. Dye-sensitized $CuAlO_2$ photocathodes for tandem solar cell applications. *J. Photon. Energy* **2011**, *1* (1), 011103.
17. Prakash, T.; Ramasamy, S. Dye Sensitized Solar Cells Using Nanocrystalline $CuAlO_2$-CuSCN Embedded Poly(vinyl carbazole) Composites as Solid Hole-Transporter. *Sci. Adv. Mater.* **2012**, *4* (1), 29–34.
18. Herraiz-Cardona, I.; Fabregat-Santiago, F.; Renaud, A.; Julián-López, B.; Odobel, F.; Cario, L.; Jobic, S.; Giménez, S. Hole conductivity and acceptor density of p-type $CuGaO_2$ nanoparticles determined by impedance spectroscopy: The effect of Mg doping. *Electrochim. Acta* **2013**, *113*, 570–574.
19. Carcia, P. F.; Shannon, R. D.; Bierstedt, P. E.; Flippen, R. B. O_2 electrocatalysis on thin film metallic oxide electrodes with the delafossite structure. *J. Electrochem. Soc.* **1980**, *127* (9), 1974–1978.
20. Hinogami, R.; Toyoda, K.; Aizawa, M.; Kawasaki, T.; Gyoten, H. Copper delafossite anode for water electrolysis. *ECS Trans.* **2013**, *58* (2), 27–31.
21. Hinogami, R.; Toyoda, K.; Aizawa, M.; Yoshii, S.; Kawasaki, T.; Gyoten, H. Active copper delafossite anode for oxygen evolution reaction. *Electrochem. Commun.* **2013**, *35* (0), 142–145.
22. Ghosh, C. K.; Popuri, S. R.; Mahesh, T. U.; Chattopadhyay, K. K. Preparation of nanocrystalline $CuAlO_2$ through sol–gel route. *J. Sol-Gel Sci. Technol.* **2009**, *52* (1), 75–81.
23. Deng, Z.; Zhu, X.; Tao, R.; Dong, W.; Fang, X. Synthesis of $CuAlO_2$ ceramics using sol-gel. *Mater. Lett.* **2007**, *61* (3), 686–689.
24. Xiong, D.; Zeng, X.; Zhang, W.; Wang, H.; Zhao, X.; Chen, W.; Cheng, Y.-B. Synthesis and characterization of $CuAlO_2$ and $AgAlO_2$ delafossite oxides through low-temperature hydrothermal methods. *Inorg. Chem.* **2014**, *53* (8), 4106–4116.
25. Sheets, W. C.; Mugnier, E.; Barnabé, A.; Marks, T. J.; Poeppelmeier, K. R. Hydrothermal synthesis of delafossite-type oxides. *Chem. Mater.* **2005**, *18* (1), 7–20.
26. Banerjee, A. N.; Maity, R.; Chattopadhyay, K. K. Preparation of p-type transparent conducting $CuAlO_2$ thin films by reactive DC sputtering. *Mater. Lett.* **2004**, *58* (1–2), 10–13.
27. Thu, T. V.; Thanh, P. D.; Suekuni, K.; Hai, N. H.; Mott, D.; Koyano, M.; Maenosono, S. Synthesis of delafossite $CuAlO_2$ p-type semiconductor with a nanoparticle-based Cu(I) acetate-loaded boehmite precursor. *Mater. Res. Bull.* **2011**, *46* (11), 1819–1827.

28. Kumekawa, Y.; Hirai, M.; Kobayashi, Y.; Endoh, S.; Oikawa, E.; Hashimoto, T. Evaluation of thermodynamic and kinetic stability of $CuAlO_2$ and $CuGaO_2$. *J. Therm. Anal. Calorim.* **2010**, *99* (1), 57–63.
29. Amrute, A. P.; Łodziana, Z.; Mondelli, C.; Krumeich, F.; Pérez-Ramírez, J. Solid-state chemistry of cuprous delafossites: Synthesis and stability aspects. *Chem. Mater.* **2013**, *25* (21), 4423–4435.
30. Taurino, I.; Carrara, S.; Giorcelli, M.; Tagliaferro, A.; De Micheli, G. Comparison of two different carbon nanotube-based surfaces with respect to potassium ferricyanide electrochemistry. *Surf. Sci.* **2012**, *606* (3–4), 156–160.
31. Min-Jung, S.; Dong-Hwa, Y.; Joon-Hyung, J.; Nam-Ki, M.; Suk-In, H. Comparison of effective working electrode areas on planar and porous silicon substrates for cholesterol biosensor. *Jap. J. Appl. Phys.* **2006**, *45* (9R), 7197.
32. Aljabali, A. A. A.; Barclay, J. E.; Butt, J. N.; Lomonossoff, G. P.; Evans, D. J. Redox-active ferrocene-modified Cowpea mosaic virus nanoparticles. *Dalton Trans.* **2010**, *39* (32), 7569–7574.
33. Singh, M. K.; Dussan, S.; Sharma, G. L.; Katiyar, R. S. Raman scattering measurements of phonon anharmonicity in $CuAlO_2$ thin films. *J. Appl. Phys.* **2008**, *104* (11).
34. Ingram, B. J.; Mason, T. O.; Asahi, R.; Park, K. T.; Freeman, A. J. Electronic structure and small polaron hole transport of copper aluminate. *Phys. Rev. B* **2001**, *64* (15), 155114.
35. Pellicer-Porres, J.; Martínez-García, D.; Segura, A.; Rodríguez-Hernández, P.; Muñoz, A.; Chervin, J. C.; Garro, N.; Kim, D. Pressure and temperature dependence of the lattice dynamics of $CuAlO_2$ investigated by Raman scattering experiments and ab initio calculations. *Phys. Rev. B* **2006**, *74* (18), 184301.
36. Ahmed, J.; Trinh, P.; Mugweru, A. M.; Ganguli, A. K. Self-assembly of copper nanoparticles (cubes, rods and spherical nanostructures): Significant role of morphology on hydrogen and oxygen evolution efficiencies. *Solid State Sci.* **2011**, *13* (5), 855–861.
37. Ahmed, J.; Ganguly, A.; Saha, S.; Gupta, G.; Trinh, P.; Mugweru, A. M.; Lofland, S. E.; Ramanujachary, K. V.; Ganguli, A. K. Enhanced electrocatalytic activity of copper–cobalt nanostructures. *J. Phys. Chem. C* **2011**, *115* (30), 14526–14533.
38. Kumar, B.; Saha, S.; Ganguly, A.; Ganguli, A. K. A facile low temperature (350 °C) synthesis of Cu_2O nanoparticles and their electrocatalytic and photocatalytic properties. *RSC Adv.* **2014**, *4* (23), 12043–12049.